ChemComm

Electrolyte screening studies for Li metal batteries

Journal:	*ChemComm*
Manuscript ID	CC-COM-06-2020-004354.R1
Article Type:	Communication

COMMUNICATION

Electrolyte screening studies for Li metal batteries

Jeesoo Seok[a], Na Zhang[a], Burak Ulgut[b], Aihua Jin[c], Seung-Ho Yu*[c] and Héctor D. Abruña*[a]

Received 00th January 20xx,
Accepted 00th January 20xx

DOI: 10.1039/x0xx00000x

From 60 solvent electrolyte combinations tested, we find that Li metal anodes, tested in 1 M LiFSI in DOL:DME exhibit an outstanding cycling performance (>500 cycles) even at high current densities (3 mA/cm^2). The excellent performance is abscribed, at least in part, to a low Li nucleation overpotential and a low charge transfer resistance during cycling.

There is a great demand for high performance rechargeable batteries for portable electronic devices and electric vehicles[1]. Lithium metal batteries represent one of the most promising candidates for next-generation rechargeable batteries due to their very high theoretical capacity (3862 mAh/g) and wide operating voltage window[2,3]. Using a lithium metal anode for Li–S batteries would maximize the capacity of sulfur as a cathode, with high energy density. However, due to its inherent instability [4], utilization of lithium metal as an anode has remained elusive. During the lithium plating process, lithium metal can react with electrolyte solution components, forming a solid-electrolyte interphase (SEI) layer. Lithium also tends to form dendrites, which can lead to catastrophic failure[2]. Because of the large volumetric changes of plated lithium, the SEI layer cracks during cycling, exposing fresh lithium which, in turn, reacts with the electrolyte, leading to the formation of a new SEI layer[5]. As the battery is cycled, lithium metal is continuously consumed, leading to a low Coulombic efficiency.

To suppress dendritic growth, various strategies have been proposed including developing a stable artificial SEI layer[6-9] that protects fresh lithium from exposure to the electrolyte, introducing electrolyte additives that help form a stable SEI layer[10, 11], distributing lithium ions using nanochannels that promote homogeneous deposition of lithium[12, 13], controlling lithium ion flux using carbon composites that provide strong mechanical properties as well as chemical stability[14, 15], and utilizing highly concentrated electrolytes to control SEI layer and suppress dendritic growth of lithium[16, 17]. While some of these strategies appear promising, the above-mentioned issues persist and/or look infeasible due to their high cost for commercialization. Thus, a fundamental study of commonly used electrolytes is necessary in order better understand the causes of dendrite formation and growth.

In this work, we have tested lithium metal anodes using a commercial lithium foil with different electrolytes containing lithium perchlorate ($LiClO_4$), lithium hexafluorophosphate ($LiPF_6$), lithium bis(trifluoromethane)sulfonimide (LiTFSI) and lithium bis(fluorosulfonyl)imide (LiFSI) in various carbonate- or ether-based solvents. (See S.I.) Of these, three different electrolytes were chosen for further analysis using scanning electron microscopy (SEM), X-ray photoelectron spectroscopy (XPS) and impedance methods. When LiFSI is used in ether-based solvents, the nucleation overpotential was significantly lowered and both lithium/lithium symmetric cells and lithium–$LiFePO_4$ full cells exhibited dramatically enhanced performance, ascribed to the formation of a stable LiF layer (ostensibly serving as a surfactant layer that mediates deposition and stripping) on the surface of the lithium metal anode, as well as a low charge transfer resistance.

Li/Li symmetric cells, with different electrolytes, were tested to investigate the effects of electrolytes on the Li plating/stripping behavior (Fig. S1). Fig. 1 (a) presents the cycling performance of Li/Li symmetric cells with selected electrolytes at a current density of 3 mA/cm^2 for 1 h of each plating/stripping. Since all the cells were made with the same lithium electrode (bulk lithium metal from Alfa Aesar) on both sides, overpotentials reflect the reaction kinetics in the different electrolytes. As shown in Fig. 1 (a) and Fig. S1, cells with $LiPF_6$ or $LiClO_4$ salts, in carbonate-based solvents, exhibited a high overpotential (over 0.7 V on average). Both LiTFSI and LiFSI electrolytes in propylene carbonate (PC) exhibited high overpotentials, increasing from 0.5 V to over 2 V during cycling.

[a] Department of Chemistry and Chemical Biology, Baker Laboratory, Cornell University, Ithaca, New York 14853, United States
[b] Department of Chemistry, Bilkent University, Ankara 06800, Turkey
[c] Department of Chemical and Biological Engineering, Korea University, 145 Anam-ro, Seongbuk-gu, Seoul 02841, Republic of Korea
† Footnotes relating to the title and/or authors should appear here.
Electronic Supplementary Information (ESI) available: [details of any supplementary information available should be included here]. See DOI: 10.1039/x0xx00000x

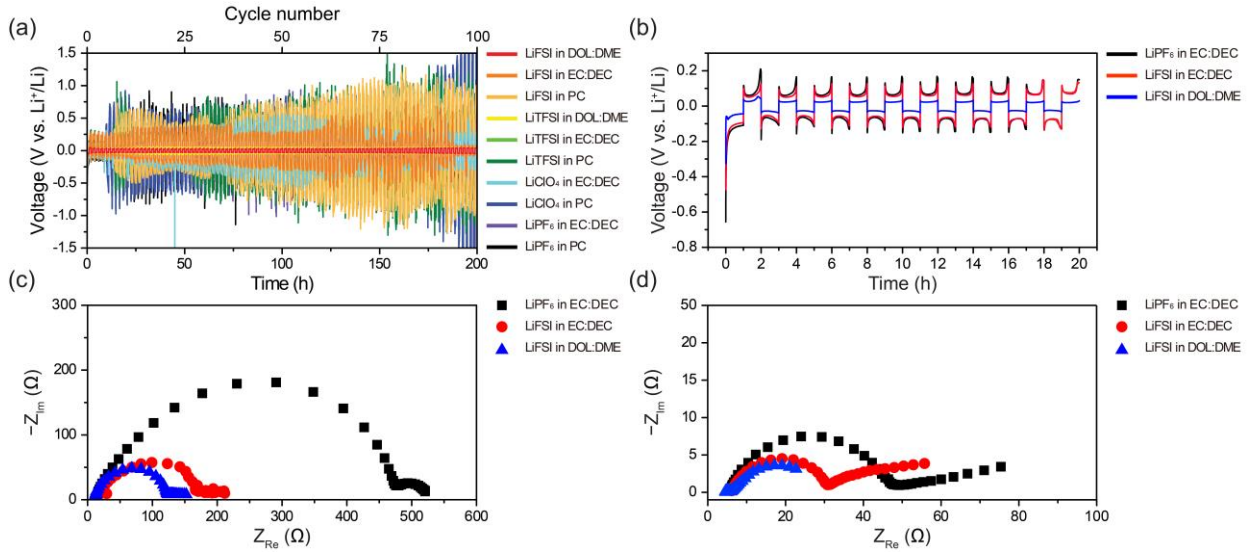

Fig. 1 (a) Lithium plating/stripping tests in Li/Li symmetric cells with commercial lithium at a current density of 3 mA/cm^2 in different electrolytes, (b) electrochemical cycling performance of Li/Li symmetric cells the cells in $LiPF_6$ in EC:DEC, LiFSI in EC:DEC, and LiFSI in DOL:DME and Nyquist plots for EIS data collected (c) before and (d) after cycling Li/Li symmetric cells, respectively.

However, cells with LiTFSI and LiFSI salts in ethylene carbonate (EC):diethyl carbonate (DEC) solvents exhibited an improved performance with a relatively low overpotential (<0.5 V). More importantly, when a mixture of 1,3-dioxolane (DOL): dimethyl ether (DME) was used as a solvent for both salts, the cycling performance of the symmetric cells was dramatically improved with a very low overpotential of ~30 mV. The cell with LiFSI in DOL:DME had the lowest overpotential among all the studied samples. Lithium bis(oxalato)borate (LiBOB) electrolytes exhibited poor cycling performance compared to others. Electrolytes with lithium tetrafluoroborate ($LiBF_4$) showed slightly better performance compared to LiBOB, however, the overpotential during lithium stripping/plating processes were, on overage, over 300 mV. Both LiBOB and $LiBF_4$ did not show stable cycling performance regardless of which solvents were used. When mixed salts were used as an electrolyte, there was a gradual increase in the magnitude of the overpotential. Among mixed salts electrolytes, the combinations of $LiPF_6$:LiFSI and $LiPF_6$:LiTFSI in EC:DMC or EC:DEC showed improved performance when compared to $LiPF_6$ electrolytes, however, LiFSI or LiTSFI electrolytes showed much enhanced cycling performance with consistently low overpotentials.

In order to understand the improved cycling performance of cells with LiFSI in DOL:DME, we chose three different systems (cells with $LiPF_6$ in EC:DEC, LiFSI in EC:DEC and LiFSI in DOL:DME) for further characterization.

Fig. 1 (b) shows the voltage profiles for the first 20 alternating current pulses for $LiPF_6$ in EC:DEC, LiFSI in EC:DEC and LiFSI in DOL:DME. When a constant current density of 3 mA/cm^2 was applied, initial nucleation occurs at the lithium electrode on the positive side while dissolution takes place at the lithium metal electrode on the negative side. During the initial plating, the overpotential was the highest, so very sharp (transient) peaks are observed in the voltage profile. This is generally referred to as "nucleation overpotential"[4], since a higher voltage is required for nucleation, compared to the subsequent growth processes. As shown in Fig. 1 (b), the nucleation overpotentials were 0.66 V, 0.47 V, and 0.32 V for $LiPF_6$ in EC:DEC, LiFSI in EC:DEC and LiFSI in DOL:DME electrolytes, respectively. The overpotentials decreased continuously during the initial 30 mins of cycling and then stabilized to 0.11 V, 0.09 V and 0.04 V, respectively. When a reverse current was applied, a plateau, with two distinct peaks, appeared for all electrolytes. The first peak appeared right after the direction of the current was reversed, where the overpotentials were 0.12 V, 0.10 V, and 0.04 V for $LiPF_6$ in EC:DEC, LiFSI in EC:DEC and LiFSI in DOL:DME electrolytes, respectively. These values reflect another nucleation process, occurring on the lithium electrode on the negative side, and were greatly diminished when compared to the initial nucleation overpotential. This behavior is likely due to defects on the lithium metal surface generated during the first dissolution cycle. It is well known that nucleation processes are favored at defect sites because they often act as nucleation sites[18]. Thus, the magnitude of the nucleation overpotentials, for all electrolytes, decreased when the reaction was reversed. A second peak started to arise after applying the reverse current for 0.6 h. This increase in the overpotential could be attributed to the bulk lithium dissolution processes. Once all of the electrochemically active lithium that was previously plated was consumed, bulk lithium started to be stripped, which increased the overpotential[4]. As lithium was continuously removed from the bulk lithium, the overpotentials for all three systems decreased.

While all three electrolytes behaved similarly, the magnitude of the overpotentials varied depending on the identity of the solvents and salts used. The differences could be ascribed to the electrolyte conductivity and lithium ion diffusion rates, which were evaluated by electrochemical impedance spectroscopy (EIS). EIS analysis (Fig. 1 (c)) showed that LiFSI in DOL:DME electrolyte had the highest electrolyte conductivity and fastest lithium ion migration through the solid-electrolyte interface (SEI) layer. While the EIS analysis was complicated by instabilities; the high frequency semicircle was consistently

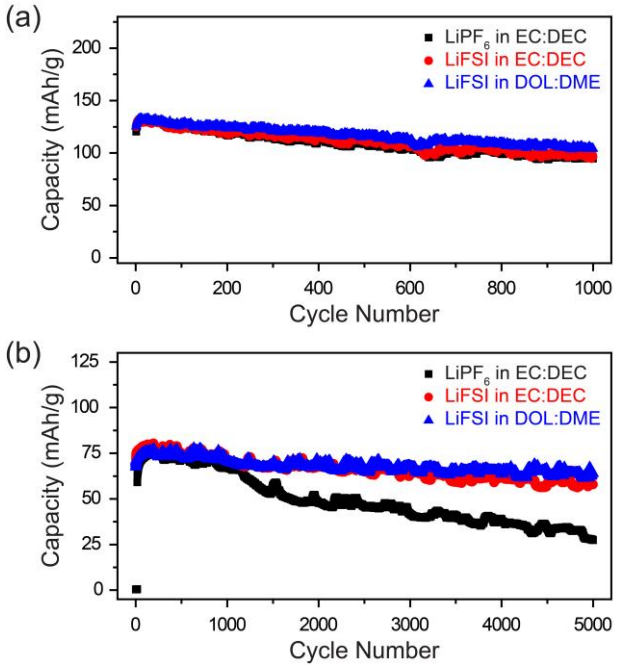

Fig. 2 Electrochemical performance of lithium metal batteries employing a commercial LFP cathode and a commercial Li metal anode in different electrolytes (a) at 1 C and (b) with a current density of 3 mA/cm^2 .

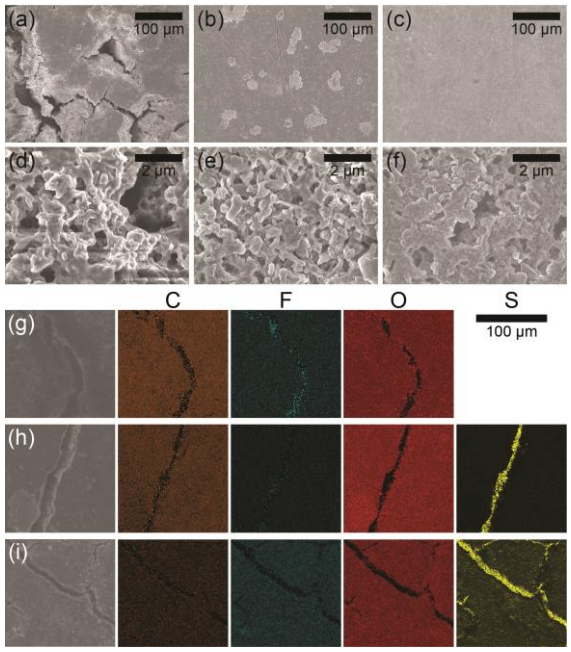

Fig. 3 SEM images and corresponding EDX mapping results (C: orange, F: cyan, O: red and S: yellow) of lithium metal electrodes after 5000 cycles in full cells in (a, d, g) $LiPF_6$ in EC:DEC, (b, e, h) LiFSI in EC:DEC, and (c, f, i) LiFSI in DOL:DME.

stable on all data sets. Based on the literature[19], it is clear that the high frequency semicircle can be attributed to the properties of the SEI layer. In all three samples, the capacitance of the layer increased and the charge transfer resistance across the layer decreased upon cycling (Fig. 1 (c, d)). This indicates that the electrodes got rougher through the cycling process. As expected, the resistance, both before and after cycling, was well matched with the cycling performance of the (Li/Li) symmetric cells. Further, upon cycling, the sample that exhibited the largest decrease in resistance was the LiFSI in DOL:DME system (Fig. S2, Table S1).

To assess the performance of these electrolytes in practical systems, full cells based on a commercial LFP (lithium iron phosphate, Fig. S3) cathode and a commercial Li foil as an anode were tested in $LiPF_6$ in EC:DEC, LiFSI in EC:DEC, and LiFSI in DOL:DME (2.5–4.0 V vs. Li^+/Li) (Fig. 2). The initial capacities for all solvent/salt combinations cycled at 1 C rate (1 C =175 mA/g) were comparable to each other. The combination employing LiFSI in DOL:DME showed slightly better cycling stability with a capacity retention of 83%, while the capacity retention of $LiPF_6$ in EC:DEC was 79% and that of LiFSI in EC:DEC was 77% after 1000 cycles (Fig. 2 (a)).

In order to study the electrochemical performance at high C-rates, all cells were cycled at a current density of 3 mA/cm^2 which was the same value as in symmetric cell tests, corresponding to about 10 C, with an areal mass loading of about 1.9 mg/cm^2. As shown in Fig. 2 (b), the cycling stability at 10 C showed the same trend as in the tests at 1 C, even though the initial capacities vary slightly due to the different C rates. Regardless of the initial capacities, the full cells tested in LiFSI in DOL:DME exhibited the highest stability even at high current densities. Interestingly, all batteries required an activation process, which is likely due to the high current density employed, as they delivered lower capacities for the first 150 cycles. In particular, the cell in $LiPF_6$ in EC:DEC was not able to deliver any reversible capacity until the 17th cycle. Therefore, the capacity retention of all cells was calculated based on the capacity at the 150th cycle. The capacity retentions of full cells with LFP cathodes in $LiPF_6$ in EC:DEC, LiFSI in EC:DEC and LiFSI in DOL:DME were 37%, 73% and 84%, respectively, after 5000 cycles at a current density of 3 mA/cm^2. Regardless of the C rates, full cells in LiFSI in DOL:DME showed superior performance in terms of capacity and stability. These results are in good agreement with their Coulombic efficiencies (CEs). Asymmetric cells with Cu and Li foils were tested in $LiPF_6$ in PC, $LiPF_6$ in EC:DEC, LiFSI in EC:DEC, and LiFSI in DOL:DME (Fig. S4). The cell cycled with $LiPF_6$ in PC showed the most unstable cycling performance. $LiPF_6$ in EC:DEC and LiFSI in EC:DEC also showed unstable performance after 16th cycle and 33rd cycle, respectively, whereas the cell cycled with LiFSI in DOL:DME showed excellent stability throughout 50 cycles. As expected, CEs of the cell with LiFSI in DOL:DME outperformed the rest (Fig. S5).

In order to elucidate the effects of the electrolytes, the surface morphology of the lithium electrodes after 5000 cycles, in a full cell, was characterized by SEM. As shown in Fig. 3 (a, d), massive cracking was observed on the surface of the lithium electrode cycled in $LiPF_6$ in EC:DEC and the plated lithium layer was more porous than in the other two electrodes. On the other hand, lithium electrodes cycled in LiFSI in EC:DEC or DOL:DME, exhibited surfaces that were relatively flat and denser (Fig. 3 (b, c, e, f)). The components of the SEI layer were confirmed by EDX elemental mapping. As shown in Fig. 3 (g–i), in the case of lithium electrodes cycled in $LiPF_6$ in EC:DEC and LiFSI in EC:EC, all salt components were detected from the cracked area, while the signals of fluoride, from lithium electrodes cycled in LiFSI in

DOL:DME, were found on the surface of the electrode, indicating that F (fluorine) is a major component of the SEI layer of lithium electrodes in LiFSI in DOL:DME.

To further understand the compositions of the SEI layers, XPS measurements were performed for lithium electrodes cycled in LiFSI in EC:DEC and LiFSI in DOL:DME (Fig. S6). In Fig. S6 (b), two main components were detected at 687.9 eV and 684.9 eV in the F 1*s* region of LiFSI in EC:DEC, whereas only one peak at 684.9 eV appeared in the F 1*s* region of LiFSI in DOL:DME (Fig. S6 (e)). The peak at 684.9 eV is known to be LiF or F^-, which could be attributed to the decomposition of LiFSI into LiF[20]. According to previous studies, LiF layers can suppress dendritic growth of lithium upon cycling as it can act as a surfactant and guide lithium growth by providing preferential paths to lithium ions[9]. Therefore, the formation of LiF during cycling yields a stable SEI layer on lithium electrodes in LiFSI in DOL:DME, preventing continuous electrolyte decomposition. On the other hand, the new peak at 687.9 eV in LiFSI in EC:DEC indicates that fluorides in LiFSI are decomposed into two different species, LiF and CF_3[20]. The CF_3 radicals from LiFSI are thermodynamically/kinetically unstable and are most reactive by nature. Such high reactivity would interfere with the formation of a stable SEI layer during reaction, leading to continuous consumption of metal and electrolytes. Several peaks at 289.6, 286.3 and 284.5 eV, ascribed to CH_2–CF_2, C–O and C–C/H, respectively, were detected in the C 1*s* region in the sample cycled in LiFSI in EC:DEC[19] (Fig. S6 (c)), as CF_3 radicals could react with other solvent or salt molecules. However, only one peak at 284.5 eV was observed for C 1*s* from the electrode cycled in LiFSI in DOL:DME as shown in Fig. S6 (f). Based on XPS results, a salt–solvent mixture of LiFSI and EC:DEC produces lithium fluoride as well as CF_3 radicals upon cycling, leading to continuous electrolyte consumption via serial side reactions. As a result, various carbon components were detected in the C 1*s* spectra. A combination of LiFSI in DOL:DME generates a LiF layer on the surface of the lithium electrode during cycling and forms a stable SEI layer, suppressing electrolyte decomposition.

In conclusion, lithium/lithium symmetric cells and full cells were tested in various electrolytes to study their behavior with particular emphasis on the deposition/stripping of lithium metal. Among the numerous electrolytes studied, LiFSI in DOL:DME showed the lowest nucleation overpotential, and EIS results suggest that it has the lowest charge transfer resistance during cycling. A full cell tested with LiFSI in DOL:DME showed superior cycling stability both at 1 C and a current density of 3 mA/cm^2 compared to $LiPF_6$ in EC:DEC and LiFSI in EC:DEC. Its excellent performance can be attributed to the formation of a LiF layer and the absence of CF_3 radicals on the Li surface as a stable SEI layer, preventing further decomposition of the electrolyte and solvent.

Ongoing and future work will focus on a mechanistic and kinetic understanding of the processes involved.

Acknowledgements

This work is supported by a generous gift from alpha-En corp. This work made use of the Cornell Center for Materials Research Shared Facilities which are supported through the NSF MRSEC program (DMR-1719875). S.-H.Y. acknowledges the support by the National Research Foundation of Korea (NRF) grant funded by the Korea government (MSIT) (NRF-2020R1C1C1012308). A. J. acknowledges the support by the National Research Foundation of Korea (NRF) grant funded by the Korea government (MSIT) (NRF-2020R1A2C1012342).

Conflicts of interest

There are no conflicts to declare.

References

1. J. M. Tarascon and M. Armand, *Nature*, 2001, **414**, 359-367.
2. W. Xu, J. Wang, F. Ding, X. Chen, E. Nasybulin, Y. Zhang and J.-G. Zhang, *Energy Environ. Sci.*, 2014, **7**, 513-537.
3. X.-B. Cheng, R. Zhang, C.-Z. Zhao and Q. Zhang, *Chem. Rev.*, 2017, **117**, 10403-10473.
4. K. N. Wood, E. Kazyak, A. F. Chadwick, K.-H. Chen, J.-G. Zhang, K. Thornton and N. P. Dasgupta, *ACS Cent. Sci.*, 2016, **2**, 790-801.
5. Q. Zhang, Y. Lu, L. Miao, Q. Zhao, K. Xia, J. Liang, S.-L. Chou and J. Chen, *Angew. Chem. Int. Ed.*, 2018, **57**, 14796-14800.
6. Y. Nan, S. Li, B. Li and S. Yang, *Nanoscale*, 2019, **11**, 2194-2201.
7. J. Lang, Y. Long, J. Qu, X. Luo, H. Wei, K. Huang, H. Zhang, L. Qi, Q. Zhang, Z. Li and H. Wu, *Energy Storage Mater.*, 2019, **16**, 85-90.
8. W. Liu, W. Li, D. Zhuo, G. Zheng, Z. Lu, K. Liu and Y. Cui, *ACS Cent. Sci.*, 2017, **3**, 135-140.
9. Y. Yuan, F. Wu, Y. Bai, Y. Li, G. Chen, Z. Wang and C. Wu, *Energy Storage Mater.*, 2019, **16**, 411-418.
10. Y. Zhang, J. Qian, W. Xu, S. M. Russell, X. Chen, E. Nasybulin, P. Bhattacharya, M. H. Engelhard, D. Mei, R. Cao, F. Ding, A. V. Cresce, K. Xu and J.-G. Zhang, *Nano Lett.*, 2014, **14**, 6889-6896.
11. P. Shi, L. Zhang, H. Xiang, X. Liang, Y. Sun and W. Xu, *ACS Appl. Mater. Interfaces*, 2018, **10**, 22201-22209.
12. W. Liu, D. Lin, A. Pei and Y. Cui, *J. Am. Chem. Soc.*, 2016, **138**, 15443-15450.
13. H. Fan, Q. Dong, C. Gao, H. Jiang, B. Hong and Y. Lai, *J. Electroanal. Chem.*, 2019, **839**, 231-237.
14. G. Zheng, S. W. Lee, Z. Liang, H.-W. Lee, K. Yan, H. Yao, H. Wang, W. Li, S. Chu and Y. Cui, *Nat. Nanotechnol.*, 2014, **9**, 618.
15. R. Zhang, X. Chen, X. Shen, X.-Q. Zhang, X.-R. Chen, X.-B. Cheng, C. Yan, C.-Z. Zhao and Q. Zhang, *Joule*, 2018, **2**, 764-777.
16. M. Wang, L. Huai, G. Hu, S. Yang, F. Ren, S. Wang, Z. Zhang, Z. Chen, Z. Peng, C. Shen and D. Wang, *J. Phys. Chem. C*, 2018, **122**, 9825-9834.
17. X. Fan, L. Chen, X. Ji, T. Deng, S. Hou, J. Chen, J. Zheng, F. Wang, J. Jiang, K. Xu and C. Wang, *Chem*, 2018, **4**, 174-185.
18. C. Wei, H. Fei, Y. An, Y. Tao, J. Feng and Y. Qian, *J. Mater. Chem. A*, 2019, **7**, 18861-18870.
19. J.-J. Woo, V. A. Maroni, G. Liu, J. T. Vaughey, D. J. Gosztola, K. Amine and Z. Zhang, *J. Electrochem. Soc.*, 2014, **161**, A827-A830.
20. 21. S. Jiao, X. Ren, R. Cao, M. H. Engelhard, Y. Liu, D. Hu, D. Mei, J. Zheng, W. Zhao, Q. Li, N. Liu, B. D. Adams, C. Ma, J. Liu, J.-G. Zhang and W. Xu, *Nat. Energy*, 2018, **3**, 739-746.

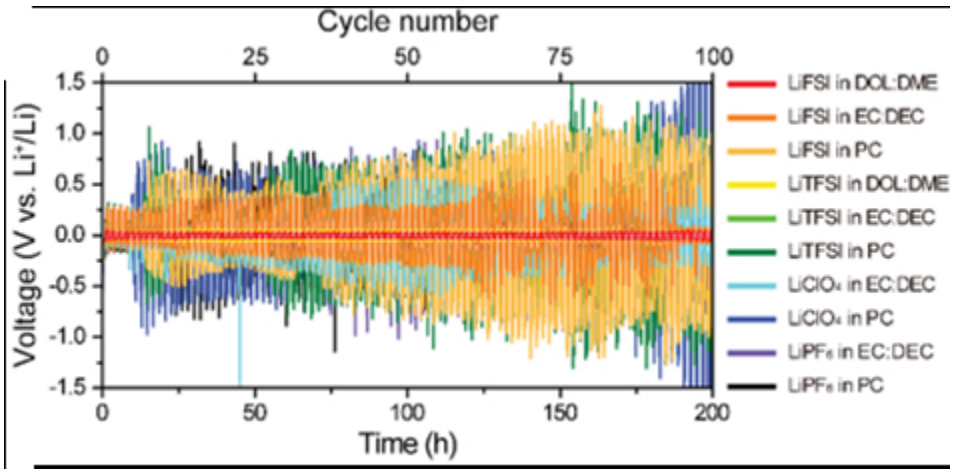

80x39mm (150 x 150 DPI)